



Article

Fabrication and Characterization of Electrochemically Deposited CuIn(Ga)Se₂ Solar Cells

Hareesh Dondapati¹ and Aswini K. Pradhan^{2,*}¹ Samsung Austin Semiconductor, 12100 Samsung Boulevard, Austin, TX 78754, USA; h.dondapati@samsung.com² Department of Physics, Hampton University, Hampton, VA 23668, USA

* Correspondence: aswini.pradhan@hamptonu.edu

Abstract: We have demonstrated a low-cost and simple method for the fabrication of large-area films using the electrodeposition technique. Fairly superior quality CuIn(Ga)Se₂ (CIGS) films were deposited by a one-step electrodeposition method using a salt bath followed by annealing in an argon atmosphere at 550 °C for 1 h. The X-ray analyses demonstrate that the films are crystalline in nature, having a chalcopyrite phase. However, the conversion efficiencies are found to be lower compared to other methods. Our results indicate that CIGS films can be produced effectively via a one-step electrodeposition method. The observed morphology can have a great impact on solar cell efficiency. With suitable modifications, this simple and cheaper manufacturing process will be the best alternative method to the vacuum deposition technique for the fabrication of reliable and flexible CIGS solar cells in the near future.

Keywords: electrodeposition; nanostructures; solar cells; multilayers

Citation: Dondapati, H.; Pradhan, A.K. Fabrication and Characterization of Electrochemically Deposited CuIn(Ga)Se₂ Solar Cells. *Nanomanufacturing* **2024**, *4*, 111–119. <https://doi.org/10.3390/nanomanufacturing4020008>

Academic Editor: Fabrizio Pirri

Received: 13 March 2024

Revised: 22 April 2024

Accepted: 20 May 2024

Published: 24 May 2024



Copyright: © 2024 by the authors. Licensee MDPI, Basel, Switzerland. This article is an open access article distributed under the terms and conditions of the Creative Commons Attribution (CC BY) license (<https://creativecommons.org/licenses/by/4.0/>).

1. Introduction

The current global energy consumption of about 10 terawatts (TW) per year is projected to exceed 30 TW by 2050; 20 TW of clean energy is needed to stabilize and compromise CO₂ concentration in the atmosphere by that time. Several clean energy technologies, such as wind, geothermal, biomass, hydroelectric, and nuclear, will play an important role in this challenge. However, none of these technologies have the scalable capacity to meet the goal of our global energy demands [1]. The current energy demand trends suggest that solar energy will play an important factor in upcoming energy production [2], as we know that direct solar energy is a huge energy resource which delivers about 4×10^{24} J of energy to the earth's surface per year (assuming a solar flux of 1 kW/m²). The world's total energy consumption is around 5.6×10^{20} J in a year [3], which means that the solar energy hitting the earth in one hour is sufficient to cover the energy needs of humanity for a whole year. For significant energy production, large-area solar cell installations are necessary. The photovoltaic (PV) market is now dominated by crystalline silicon solar cells. The continuous increase in the demand for PV modules and the need for low-cost PV options have pushed these types of cells to the limit and created some disadvantages for c-Si technology, such as the costly processing of materials and device fabrication steps. These have shifted recent commercial interest towards thin-film solar cells [4]. Compared to wafer-based Si technology, thin-film solar cells are cost-effective to deposit on large-area substrates, such as (soda-lime) glass [5], stainless steel, or even polyimide sheets, which would make these solar cells truly lightweight by saving the materials' manufacturing time and the weight of the modules, which is of interest in favoring thin-film solar cells.

The absorber layers used in thin-film solar cells are generally polycrystalline in nature, deposited on electrically active or passive substrates, such as soda-lime glasses, plastics, ceramics, steel, or silicon substrates. Among all materials, amorphous Si (a-Si),

polycrystalline Si (p-Si), CuIn(Ga)Se₂ (CIGS), and CdTe/CdS are the most promising. In particular, CIGS and CdTe show the appropriate direct band gap, allowing them to absorb solar radiation much more efficiently than crystalline silicon. This high absorbing efficiency enables the use of only 1–10 μm thick films as the active material. CuIn_xGa_{1-x}Se₂ is one of the most promising semiconductors for the absorber layer of thin-film solar cells. Record efficiencies of up to 20.3% [6] in laboratory conditions have been obtained by the thermal co-evaporation method, as well as up to 15.7% module efficiency in mass production. However, for the wider application of these devices, manufacturing process optimization and cost reduction are very much needed. Hence, a lot of effort is necessary to develop new, cost-effective manufacturing technologies in order to boost cell efficiency.

Most of the labs developing CIGS films have used sputtering or co-evaporation for solar absorber fabrication, which gives independent control over elemental fluxes and process conditions such as pressure and chemical atmosphere. However, these and other techniques involving high vacuums have several economic problems. The deposition systems create a large capital cost, and the use of vacuum deposition is highly energy intensive. In addition, material utilization is not optimal in these techniques, reaching a maximum of 80% with even the most efficient sputtering systems. Hence, there is a need to identify lower-cost processing methods for high-yield CIGS film growth for high-efficiency solar cells. One of the promising methods is electrodeposition, which is a low-cost method that has been explored for CIS and CIGS film formation. The electrodeposition approach concentrates on the deposition of the compound or a mixture of various Cu, In, Ga, and Se phases/elements from a single electrolyte [7,8].

The most common device structure for CIGS solar cells is shown in Figure 1. CIGS multi-junction solar cells are almost always designed in a substrate configuration. For example, it starts from soda-lime glass of a few millimeters thick, which is commonly used as a substrate. However, for lighter, thinner, and more flexible cells, substrates such as polyimide or metal foils [9] are more desirable. A thick molybdenum layer is generally used as a back contact due to its relative stability at the processing temperature, its resistance to alloying with Cu and In, and its low contact resistance to CIGS [10]. In contrast, the back contact forms Schottky barriers in CdTe-based solar cells, and represent a major hindrance due to stability issues [11]. A 1–2 μm thickness p-type CIGS absorber layer is deposited by a great variety of processes. The 10–50 nm n-type CdS buffer followed by transparent Al-doped ZnO window layers are typically deposited on top of the CIGS absorber by chemical bath deposition and the RF sputtering technique, respectively. A buffer layer of CdS has proven beneficial for device performance. ZnO layers are often utilized in a bi-layer configuration of intrinsic and Al-doped material. A less than 1 μm thick TCO (ZnO:Al) layer is used as a window layer, and on top of that, electrical contacts such as Ni/Al are deposited using a thermal evaporator.

Considering the state-of-the-art CIGS absorber-based solar cells, some films exhibit efficiencies of about 23.5% [12] (better than that of crystalline Si solar cells) and 23.4% for rigid glass substrates [13] using extensive and complex vacuum methods for depositing the absorber layers. Hence, it was suggested to consider alternative cost-effective processing or manufacturing strategies [14,15]. One of the most cost-effective, high-deposition-rate and, hence, fast production methods is the electrodeposition technique. This technique offers high material use with no electrolyte degradation, large-area substrates, and one-step deposition at room temperature.

In this paper, we report on the fabrication and characterization of multi-junction-based CIGS solar cells. We arrange the manuscript in the following way: In the Materials and Methods Section, we describe the fabrication of the Mo bottom contact followed by the study of its structural morphology and electrical conductivity and then the fabrication methods of CIGS absorber layer deposition, the CdS buffer layer, and Al:ZnO window layer deposition. In the Results and Discussion Section, we describe the microstructure, structure, composition, and electrical properties of CIGS. Finally, we summarize the results in the Results and Discussion Section.

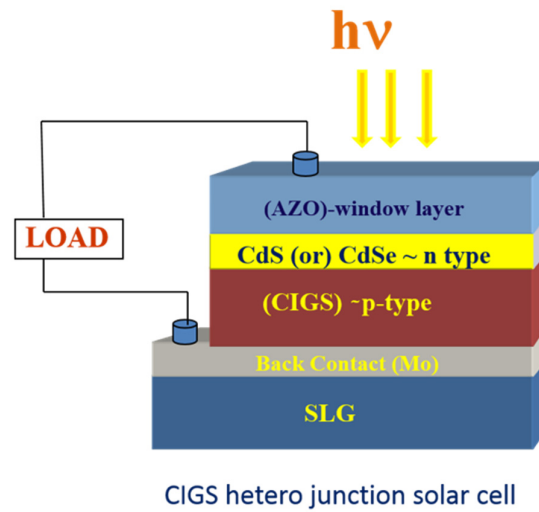


Figure 1. Structure of thin-film CIGS multi-junction solar cell.

2. Materials and Methods

Cleaning contaminants on the substrate with utmost care is a crucial step, as this has a direct impact on device performance. Soda-lime glass substrates of dimensions $4'' \times 2'' \times 2$ mm were cut using a diamond scribe followed by soaking in a bath containing de-ionized water and a cleaning agent, and they were then cleaned in an ultrasonic bath, containing a solvent like acetone and methanol, and then washed with DI water for 3 min each in order to eliminate organic impurities and some contaminants left by the cleaning agent itself. The substrates were dried using dry nitrogen before subsequent processing.

2.1. Mo Back Contact

Mo thin films were prepared on corning glass substrates using an RF magnetron sputter system using a high-purity (99.95%) 3'' Mo target. The base pressure was approximately 2×10^{-6} Torr and the flow rate of the sputtering gas (argon, 99.9999%) was initially 60 SCCM; with that, the chamber pressure was at 10 mTorr for 1 min and then changed to 20 SCCM. The rest of the deposition was kept constant at 3.2×10^{-3} Torr. The deposition was conducted at 100 W power for 1 h. The thickness was estimated using cross-sectional FESEM and determined as 90 nm.

The X-ray diffraction (XRD) of the Mo films shown in Figure 2a was carried out in a Rigaku X-ray diffractometer using $\text{CuK}\alpha$ radiation. The most intense peak at approximately $2\theta - 40^\circ$ corresponded to the $\langle 110 \rangle$ preferred orientation of BCC structure [16]. The films did not show any Mo-oxide-related peaks in this XRD study. Since better crystallized material shows sharper XRD peaks [17], and moreover, as the deposition was carried out at relatively lower working gas pressures, our growth conditions yielded highly crystalline films. After deposition, the resistivity of the samples was measured using a 4-point probe. Figure 2b shows the effect of the substrate temperature (T_s) on the temperature dependence of the electrical resistivity of grown Mo films. The figure shows a typical metallic behavior with the lowest resistivity of $9.8 \times 10^{-2} \Omega\text{-cm}$. The films showed a very small amount of residual resistivity at very low temperatures which can be related to their defects.

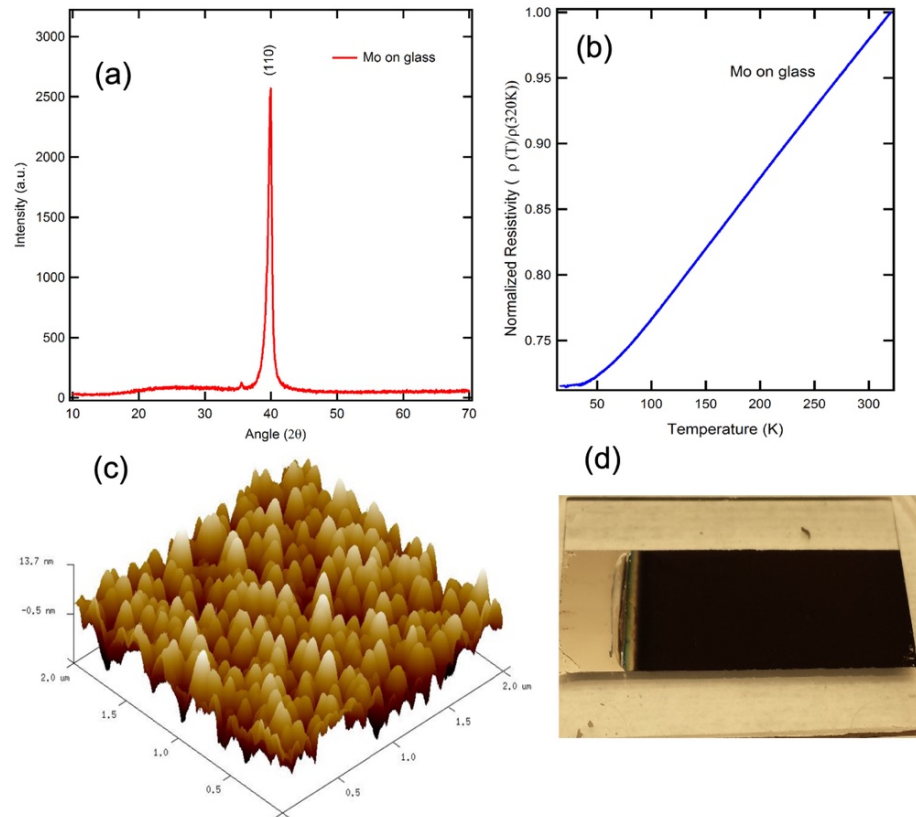


Figure 2. (a) XRD profiles of the (110) reflection of Mo, (b) plot of resistivity vs. temperature for Mo films, (c) 3D AFM image of Mo thin-film surface, and (d) CIGS thin film deposited on Mo coated glass substrate.

The surface morphology of as-deposited Mo thin films was studied by atomic force microscopy (AFM) and is shown in Figure 2c. The AFM images show a uniform distribution of grains. From Figure 2c, the presence of a dense distribution of larger grains with well-defined boundaries is clearly observed. However, the root mean square (RMS) is found to be moderately low, 4.02 nm. The planar view of the Mo films reveals that at a relatively low pressure of 3 mTorr, the films had a small, densely packed grain microstructure with closed boundaries. Since the films were grown at lower processing pressure, the energetic incident atoms impart higher momentum to the depositing Mo atoms that can fill up microvoids or vacancies, resulting in better crystallinity and enhancing grain growth. This can clearly be observed in Figure 2c. As a result of that, we were successfully able to make a pinhole-free back contact. Figure 2d shows the CIGS thin film deposited on the Mo-coated glass substrate.

2.2. CIGS Absorber Layer Deposition

CIGS thin films were electrodeposited using a classical set-up containing a three-electrode potentiostatic system in an electrochemical cell. A 900 nm Mo-coated corning glass was placed as a substrate inside the cell. The set-up comprised a reference electrode (Ag/AgCl), a counter electrode (Pt gauze), and the working electrode (Mo on glass). Mo metal was sputtered using RF magnetron sputtering with a power of 150 Watts, at room temperature. A CHI 6660 Electrochemical workstation was used for the preparation. All chemicals were analytical grade. Distilled water was used throughout. The electrochemical experiment was performed [18] in an electrodeposition bath (150 mL) to prepare the CIGS thin films on a Mo-coated surface. The chemical bath consists of a complex ion solution, containing 2.55 mM of CuCl_2 , 7.19 mM of InCl_3 , 20.7 mM of GaCl_3 , 20.7 H_2SeO_3 and

1.93 M KSCN as the complex agent. The solution was not stirred, and a potential range of -0.9 V to -0.5 V vs. Ag/AgCl was applied for 1 h at room temperature. The pH of the chemical bath was adjusted to 3 by adding drops of pH buffer solution. The obtained thin films were rinsed with bi-distilled water and dried under a nitrogen flux. The films were then thermally annealed at 550 °C for 45 min in an argon atmosphere.

2.3. CdS Buffer Layer Deposition

CdS buffer layer was deposited using the chemical bath deposition technique. The beaker was stirred modestly by a magnetic bar and put into a water bath where the temperature was kept around 68 – 70 °C. The solution inside the beaker started to turn yellowish after 3–4 min and formed CdS particles after 6–7 min. The deposition lasted for 60 min. Afterwards, the samples were rinsed with DI water and dried at room temperature. After the samples were dried out, they were annealed at 200 °C in the air for 2 min.

2.4. Al:ZnO Window Layer Deposition

Al-doped ZnO films were grown on the top of a CdS buffer layer by the RF magnetron sputtering technique from a 2 wt.% Al-doped ZnO target. The samples were deposited at the substrate temperature of 200 °C. The deposition was conducted for 1 h to reach the film thickness of 50 nm. A stainless-steel shadow mask was used to pattern the dimensions of top contacts. The 200 nm thick Al top contacts were deposited using an AJA thermal evaporator system.

3. Results and Discussions

One of the biggest challenges in depositing CIGS absorbers is to create a crack-free uniform surface throughout the substrate. The surface morphologies of CIGS films are shown in Figures 3 and 4. The effect of the pH in the bath was systematically studied. The films grown at lower pH values (2.7) not only have a non-uniform surface, as shown in Figure 3a, but cracks also formed. Upon increasing the pH value, we can clearly see that platelet-type grains form dense islands. These islands are very uniformly distributed throughout the surface of the as-grown film as shown in Figure 3b,c.

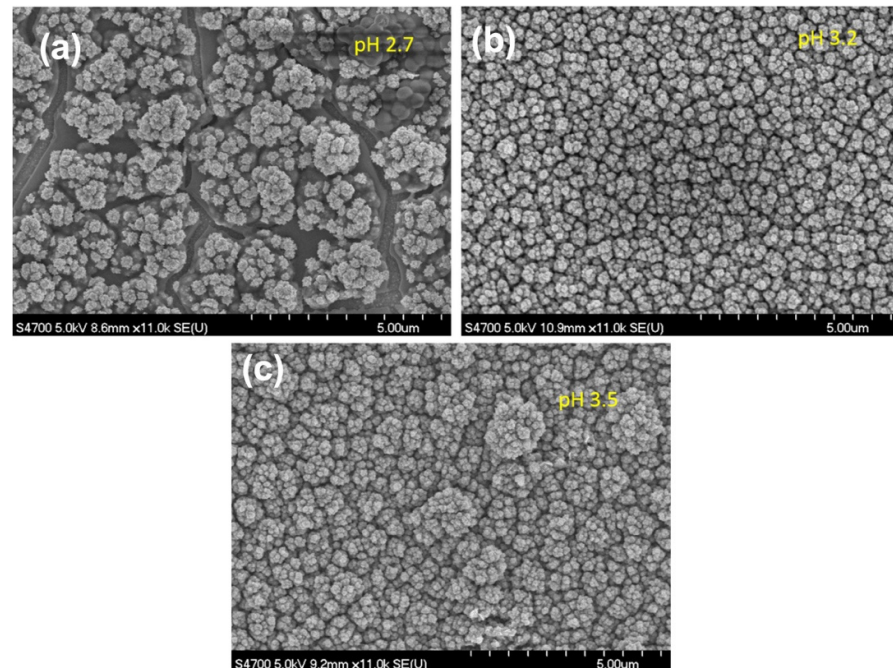


Figure 3. FESEM images of (a) as-grown and (b,c) annealed) CIGS thin films on Mo/glass.

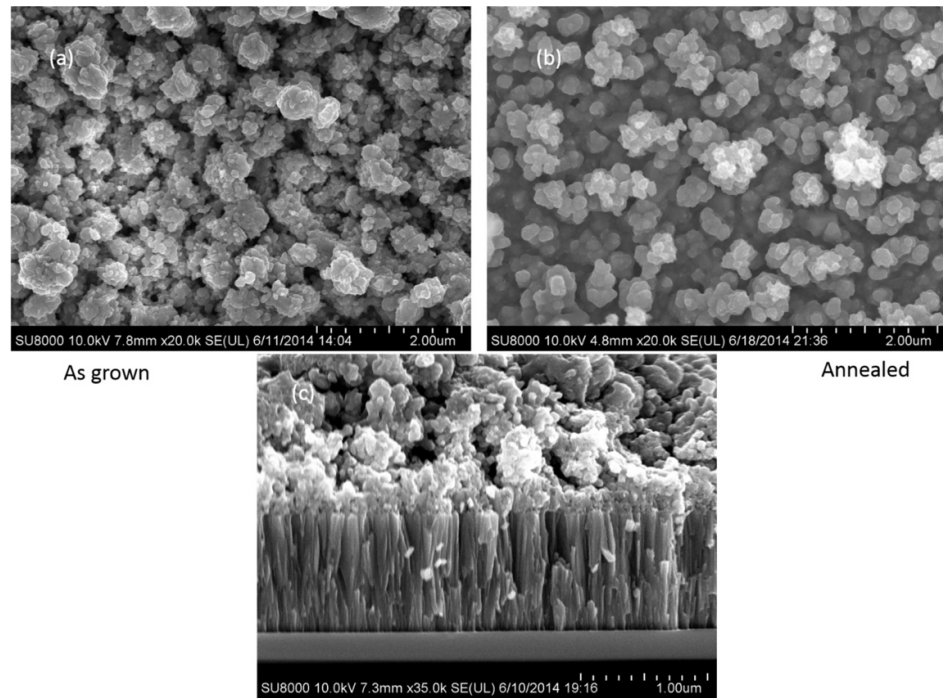


Figure 4. FESEM images of (a) as grown and (b) annealed (and (c) cross-sectional image of) CIGS thin films on Mo/glass.

The FESEM micrographs of as-deposited films (Figure 4a) show a dense and compact grain structure with some visible micro-cracks. However, upon thermal annealing, the micro-cracks disappeared, as shown in Figure 4b, indicating the effects of annealing. This may be attributed to the recrystallization of grains, consequently releasing the strain on annealing and facilitating healing of the cracks. The thermal treatment of CIGS films improves their performance [19]. The cross-sectional view (Figure 4c) of the film shows the formation of voids between the layers caused by the loss of materials. However, to improve the device efficiencies, we increase the Ga content in the absorber layer. The processing conditions are adjusted to produce void-free absorber layers with minimum material loss.

As shown in Figure 5a, all the diffraction peaks in the XRD pattern can be indexed to the chalcopyrite phase of CIGS, with an intense peak at $2\theta = 26.7^\circ$ oriented along the (112) direction [20]. Other peaks correspond to the (204) and (312) directions of the tetragonal CIGS phase [21]. The broadening and low-intensity peaks observed in the XRD pattern are due to the lack of a well-developed crystal structure of that particular phase.

The major challenge in producing these CIGS solar cells is to control film composition. EDX analyses can be used to determine the spatial distribution of the elements through the device. Figure 5b shows EDS patterns of CIGS thin films after annealing. The EDS results show that the film composition is slightly Cu-rich with respect to the CIGS composition. The composition determined using EDX refers only to a certain depth from the surface. Therefore, one can infer that the variation in the composition along the thickness axis of the films can be because of the fact that copper is deposited faster than the other elements, and the depletion of copper results in the layer being rich in another element at the other end.

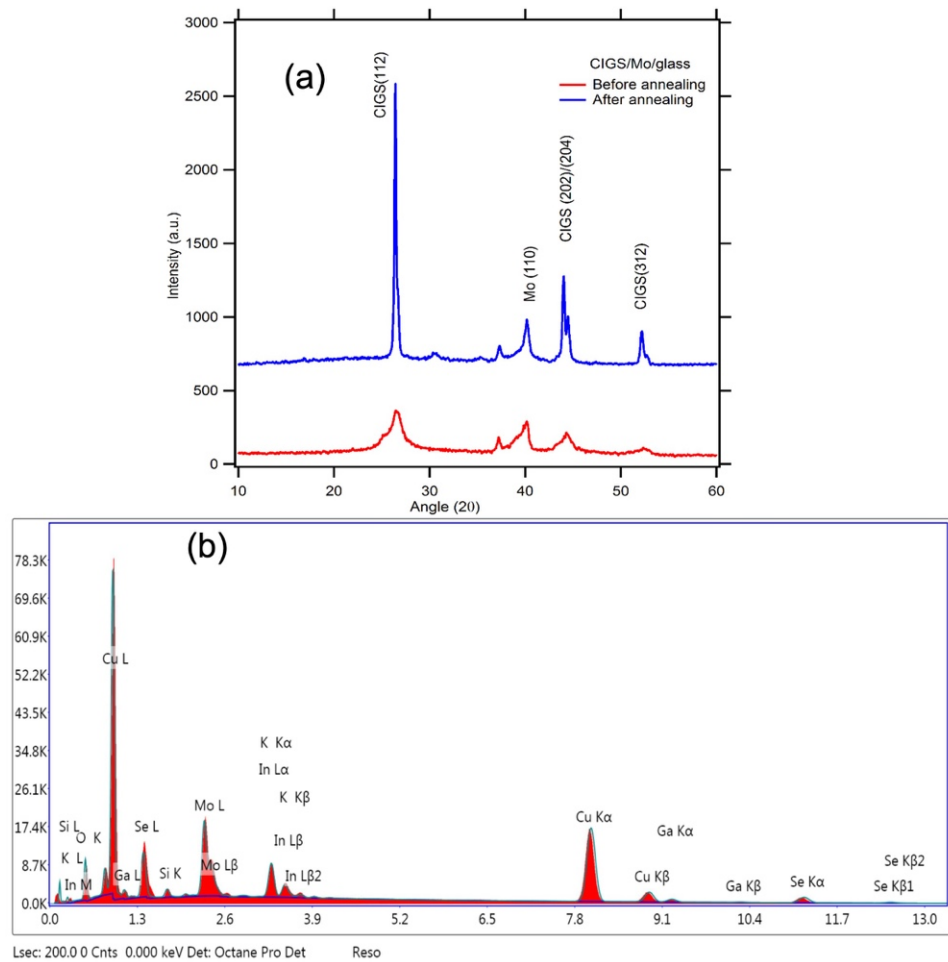


Figure 5. (a) XRD patterns of CIGS films. (b) EDX spectral analyses of the top surface of CIGS material.

The current–voltage (I–V) curves of the corresponding solar cells in the dark and under the illumination of white light are characterized using a Keithley 4200-SCS parameter analyzer connected to a probe station, and are depicted in Figure 6. The measurements are taken in the dark and under illumination with white light conditions using a CUDA lamp of 1 W/cm² intensity on 1 cm². Our dark-field measurement clearly demonstrates the Schottky barrier junction behavior at the CIGS/CdS interface and drives exciton dissociation and charge transport. In the presence of light, photovoltaic behavior is observed, and the photocurrent induced under illumination was noticeably larger, as shown in the inset of Figure 6. It is known that under reverse bias, the current is affected by light. From the FESEM images, it was seen that the absorber layer has a rougher surface as opposed to standard CIGS films, resulting in a non-uniform coverage of CdS, thus resulting in a strong leakage current observed, which again caused lower V_{oc} s of about 0.5 V on the glass substrate, with an estimated efficiency in the vicinity of 12% comparable to a recent report on CIGS-based tandem solar cells and using SiO₂ as a barrier layer [22–24]. Furthermore, because of the multi-junction solar cells, the interlayer regions need to be optimized. By further optimizing the annealing in an inert atmosphere, adjusting the composition by an appropriate potential, reducing the tetragonal phase, and tailoring the interfaces of these multi-junction solar cells, the efficiency and stability of the films can be improved.

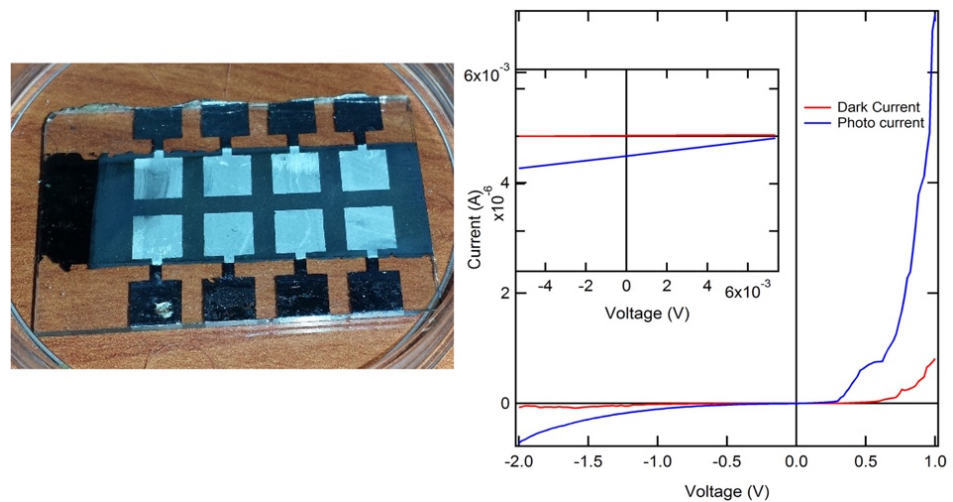


Figure 6. The solar cell devices consisting of eight active cells fabricated in the lab. The I-V characteristics of CIGS thin-film solar cells.

4. Conclusions

We have presented the most reliable and effective methods for the fabrication of CIGS solar cells. Thin films of CIGS were prepared by one-step electrodeposition in a salt bath followed by annealing in an argon atmosphere. The X-ray analyses revealed that the films are crystalline in nature with a chalcopyrite phase. Though the conversion efficiencies were by far low from our results, they clearly reveal the potential possibilities for the fabrication of flexible CIGS solar cells in the near future. It is expected that this simple and inexpensive manufacturing process may be one of the best deposition techniques compared to other methods, such as vacuum deposition, for CIGS solar cell fabrication.

Author Contributions: Funding acquisition by A.K.P.; A.K.P. and H.D. conceived the idea. H.D. conducted the experiments. H.D. and A.K.P. wrote the manuscript. All authors have read and agreed to the published version of the manuscript.

Funding: This work was supported by the National Science Foundation Centers of Research Excellence in Science and Technology (NSF-CREST) Grant Number HRD 1036494 and 1547771. The Project Director, AKP, managed all the funded projects at Norfolk State University.

Data Availability Statement: Data are contained within the article.

Acknowledgments: The authors thank R. Mundie for experimental help.

Conflicts of Interest: Author HD was employed by the company Samsung Austin Semiconductor after this was completed at Norfolk State University. The remaining authors declare that the research was conducted in the absence of any commercial or financial relationships that could be construed as a potential conflict of interest. The authors declare no conflicts of interest.

References

- Smalley, R.E. Future Global Energy Prosperity: The Terawatt Challenge. *Mrs. Bull.* **2005**, *30*, 412.
- Kaelin, M.; Rudmann, D.; Tiwari A.N. Low cost processing of CIGS thin film solar cells. *Sol. Energy* **2004**, *77*, 749.
- Lewis, N.S.; Crabtree, G.; Nozik, A.J.; Wasielewski, M.R.; Alivisatos, P.; Kung, H.; Tsao, J.; Chandler, E.; Walukiewicz, W.; Spitler, M.; et al. *Basic Research Needs for Solar Energy Utilization. Report of the Basic Energy Sciences Workshop on Solar Energy Utilization, 18–21 April 2005*; USDOE Office of Science: Washington, DC, USA, 2005.
- Graham-Rowe, D. Solar cells get flexible. *Nat. Photonics* **2007**, *1*, 433.
- Luque, A.; Hegedus, S. *Handbook of Photovoltaic Science and Engineering*, 2nd ed.; Wiley: Chichester, UK, 2011.
- Chirilă, A.; Buecheler, S.; Pianezzi, F.; Bloesch, P.; Gretener, C.; Uhl, A.R.; Fella, C.; Kranz, L.; Perrenoud, J.; Seyrling, S.; Verma, R. Highly efficient Cu (In, Ga) Se₂ solar cells grown on flexible polymer films. *Nat. Mater.* **2011**, *10*, 857.
- Long, F.; Wang, W.; Du, J.; Zou, Z. CIS (CIGS) thin films prepared for solar cells by one-step electrodeposition in alcohol solution. *J. Phys. Conf. Ser.* **2009**, *152*, 012074.

8. Kwak, W.-C.S.; Han, H.; Kim, T.G.; Sung, Y.-M. Electrodeposition of Cu (In, Ga) Se₂ crystals on high-density CdS nanowire arrays for photovoltaic applications. *Cryst. Growth Des.* **2010**, *10*, 5297.
9. Dhere, N.G. Toward GW/year of CIGS production within the next decade. *Sol. Energy Mater. Sol. Cells* **2007**, *91*, 1376.
10. Singh, U.P.; Patra, S. Progress in Polycrystalline Thin-Film Cu(In,Ga)Se₂ Solar Cells. *Int. J. Photoenergy* **2010**, *2010*, 468147. <https://doi.org/10.1155/2010/468147>.
11. Corwine, C.R.; Pudov, A.O.; Gloeckler, M.; Demtsu, S.H.; Sites, J.R. Copper inclusion and migration from the back contact in CdTe solar cells. *Sol. Energy Mater. Sol. Cells* **2004**, *82*, 481.
12. Green, M.A.; Dunlop, E.D.; Hohl-Ebinger, J.; Yoshita, M.; Kopidakis, N.; Hao, X. Solar cell efficiency tables (Version 58). *Prog. Photovolt. Res. Appl.* **2021**, *29*, 657–667. <https://doi.org/10.1002/pip.3444>.
13. Nakamura, M.; Yamaguchi, K.; Kimoto, Y.; Yasaki, Y.; Kato, T.; Sugimoto, H. Cd-free Cu (In, Ga)(Se, S)₂ thin-film solar cell with record efficiency of 23.35%. *IEEE J. Photovolt.* **2019**, *9*, 1863.
14. Bermudez, V.; Perez-Rodriguez, A. Understanding the cell-to-module efficiency gap in Cu(In,Ga)(S,Se)₂ photovoltaics scale-up. *Nat. Energy* **2018**, *3*, 466.
15. Green, M.A.; Dunlop, E.D.; Hohl-Ebinger, J.; Yoshita, M.; Kopidakis, N.; Hao, X.; Hao, X. Solar cell efficiency tables (version 57). *Prog. Photovolt.* **2020**, *28*, 629.
16. Bamiduro, O.; Chennamadhava, G.; Mundle, R.; Konda, R.; Pradhan, A.K. Synthesis and characterization of one-step electrodeposited CuIn_(1-x)Ga_xSe₂/Mo/glass films at atmospheric conditions. *Sol. Energy* **2011**, *85*, 545.
17. Scofield, J.H.; Duda, A.; Albin, D.; Ballard, B.L.; Predecki, P.K. Sputtered molybdenum bilayer back contact for copper indium diselenide-based polycrystalline thin-film solar cells. *Thin Solid Films* **1995**, *260*, 26.
18. Takahashi, A.; Pethe, S.S.; Dhere, N.G. Correlation between preparation parameters and properties of molybdenum back contact layer for CIGS thin film solar cell. In Proceedings of the 2010 35th IEEE Photovoltaic Specialists Conference, Honolulu, HI, USA, 20–25 June 2010; pp. 002478–002482.
19. Bhattacharya, R.N.; Fernandez, A.M. CuIn_{1-x}Ga_xSe₂-Based Photovoltaic Cells from Electrodeposited Precursor Films. *MRS Online Proc. Libr* **2001**, *668*, H8-10.
20. Bhattacharya, R.N.; Oh, M.K.; Kim, Y. CIGS-based solar cells prepared from electrodeposited precursor films. *Sol. Energy Mater. Sol. Cells* **2012**, *98*, 198.
21. Sastré-Hernández, J.; Calixto, M.E.; Tufiño-Velazquez, M.; Contreras-Puente, G.; Morales-Acevedo, A.; Casados-Cruz, G.; Hernández-Pérez, M.A.; Albor-Aguilera, M.L.; Mendoza-Pérez, R. Cu(In,Ga)Se₂ thin films processed by co-evaporation and their application into solar cells. *Rev. Mex. Física* **2011**, *57*, 441–445.
22. Hsu, Shu-Tsun.; Yean-San, Long.; Teng-Chun, Wu. A new method to characterize C-SI PV cell and module. In Proceedings of the 38th IEEE Photovoltaic Specialists Conference, New Orleans, LA, USA, 14-19 June 2015.
23. Hedayaty, M.; Olyae, S. High-efficiency p-n homojunction Perovskite and CIGS tandem solar cell. *Crystals* **2022**, *12*, 703.
24. Zhang, C.; Qi, T.; Wang, W.; Zhao, C.; Xu, S.; Ma, M.; Feng, Y.; Li, W.; Chen, M.; Yang, C.; et al. High efficiency CIGS solar cells on flexible stainless steel substrate with SiO₂ diffusion barrier layer. *Sol. Energy* **2021**, *230*, 1033.

Disclaimer/Publisher's Note: The statements, opinions and data contained in all publications are solely those of the individual author(s) and contributor(s) and not of MDPI and/or the editor(s). MDPI and/or the editor(s) disclaim responsibility for any injury to people or property resulting from any ideas, methods, instructions or products referred to in the content.